LETTER

doi:10.1038/nature17172

Memory retrieval by activating engram cells in mouse models of early Alzheimer's disease

Dheeraj S. Roy[1], Autumn Arons[1,2], Teryn I. Mitchell[1], Michele Pignatelli[1], Tomás J. Ryan[1,2] & Susumu Tonegawa[1,2]

Alzheimer's disease (AD) is a neurodegenerative disorder characterized by progressive memory decline and subsequent loss of broader cognitive functions[1]. Memory decline in the early stages of AD is mostly limited to episodic memory, for which the hippocampus has a crucial role[2]. However, it has been uncertain whether the observed amnesia in the early stages of AD is due to disrupted encoding and consolidation of episodic information, or an impairment in the retrieval of stored memory information. Here we show that in transgenic mouse models of early AD, direct optogenetic activation of hippocampal memory engram cells results in memory retrieval despite the fact that these mice are amnesic in long-term memory tests when natural recall cues are used, revealing a retrieval, rather than a storage impairment. Before amyloid plaque deposition, the amnesia in these mice is age-dependent[3–5], which correlates with a progressive reduction in spine density of hippocampal dentate gyrus engram cells. We show that optogenetic induction of long-term potentiation at perforant path synapses of dentate gyrus engram cells restores both spine density and long-term memory. We also demonstrate that an ablation of dentate gyrus engram cells containing restored spine density prevents the rescue of long-term memory. Thus, selective rescue of spine density in engram cells may lead to an effective strategy for treating memory loss in the early stages of AD.

AD is the most common cause of brain degeneration, and typically begins with impairments in cognitive functions[1]. Most research has focused on understanding the relationship between memory impairments and the formation of two pathological hallmarks seen in the late stages of AD: extracellular amyloid plaques and intracellular aggregates of tau protein[1,2]. The early phases of AD have received relatively less attention, although synaptic phenotypes have been identified as major correlates of cognitive impairments in both human patients and mouse models[3,6]. Several studies have suggested that the episodic memory deficit of AD patients is due to ineffective encoding of new information[7–9]. However, since the cognitive measures used in these studies rely on memory retrieval, it is not possible to discriminate rigorously between impairments in information storage and disrupted retrieval of stored information. This issue has an important clinical implication: if the amnesia is due to retrieval impairments, memory could be restored by technologies involving targeted brain stimulation.

A mouse model of AD (hereafter referred to as 'AD mice')[10] overexpresses the delta exon 9 variant of presenilin 1 (PS1; also known as PSEN1), in combination with the Swedish mutation of β-amyloid precursor (APP). Consistent with previous reports[3–5], 9-month-old AD mice showed severe plaque deposition across multiple brain regions (Fig. 1a), specifically in the dentate gyrus (DG) (Fig. 1b) and medial entorhinal cortex (EC) (Fig. 1c); in contrast, 7-month-old AD mice lacked amyloid plaques (Fig. 1d and Extended Data Fig. 1a–d). Focusing on these two age groups of AD mice, we quantified short-term (1 h; STM) and long-term (24 h; LTM) memory formation using contextual fear conditioning (CFC) (Fig. 1e). Nine-month-old AD mice were impaired in both STM and LTM, which suggested a deficit in memory encoding (Fig. 1k–o). By contrast, 7-month-old AD mice showed normal levels of training-induced freezing (Fig. 1f) and normal STM (Fig. 1g), but were impaired in LTM (Fig. 1h). Neither control nor 7-month-old AD mice displayed freezing behaviour in a neutral context (Fig. 1i). In the DG of 7-month-old AD mice, the levels of cells that were immediate early gene c-Fos-positive after CFC training were normal, but were lower compared with control mice after LTM tests (Fig. 1j). Motor behaviours and the density of DG granule cells were normal in these mice (Extended Data Fig. 1e–k). Thus, these behavioural- and cellular-level observations confirmed that 7-month-old AD mice serve as a mouse model of early AD regarding memory impairments.

Recently, molecular, genetic and optogenetic methods to identify neurons that hold traces, or engrams, of specific memories have been established[11,12]. Using this technology, several groups have demonstrated that DG neurons activated during CFC learning are both sufficient[11–14] and necessary[15] for subsequent memory retrieval. In addition, our recent study found that engram cells under protein-synthesis-inhibitor-induced amnesia were capable of driving acute memory recall if they were directly activated optogenetically[14]. Here, we applied this memory engram cell identification and manipulation technology to 7-month-old AD mice to determine whether memories could be retrieved in the early stages of the disease. Because it is known that the EC–hippocampus (HPC) network is among the earliest to show altered synaptic/dendritic properties and these alterations have been suggested to underlie the memory deficits in early AD[16,17], we focused on labelling the DG component of CFC memory engram cells of 7-month-old AD mice using a double adeno-associated virus (AAV) system (Fig. 1p, q and Methods). Although on a doxycycline (DOX) diet DG neurons completely lacked channelrhodopsin 2 (ChR2)–enhanced yellow fluorescent protein (eYFP) labelling, 1 day off DOX was sufficient to permit robust ChR2–eYFP expression in control mice (Fig. 1r, s and Extended Data Fig. 2a–c), as well as in 7-month-old AD mice (Fig. 1t, u).

As expected, these engram-labelled early AD mice were amnesic a day after CFC training (Fig. 1v). But, remarkably, these mice froze on the next day in a distinct context (context B) as robustly as equivalently treated control mice in response to blue light stimulation of the engram cells (Fig. 1w). This light-specific freezing was not observed using on-DOX mice (Extended Data Fig. 2d–f). A natural recall test conducted on the third day in the conditioning context (context A) revealed that the observed optogenetic engram reactivation did not restore memory recall by natural cues in early AD mice (Fig. 1x). This was the case even after multiple rounds of light activation of the engram cells (Extended Data Fig. 3). We replicated the successful optogenetic rescue of memory recall in two other models of early AD: a triple transgenic line obtained by mating *c-Fos-tTA* mice with double-transgenic APP/PS1 mice (Extended Data Fig. 4a–g) and a widely used triple-transgenic AD model[18] (PS1/APP/tau (also known as MAPT); Extended Data Fig. 4h–m). These data show that DG engram cells in 7-month-old mouse models of early AD are sufficient to induce memory recall upon optogenetic reactivation, which indicates a deficit of memory retrievability during early AD-related memory loss.

[1]RIKEN-MIT Center for Neural Circuit Genetics at the Picower Institute for Learning and Memory, Department of Biology and Department of Brain and Cognitive Sciences, Massachusetts Institute of Technology, Cambridge, Massachusetts 02139, USA. [2]Howard Hughes Medical Institute, Massachusetts Institute of Technology, Cambridge, Massachusetts 02139, USA.

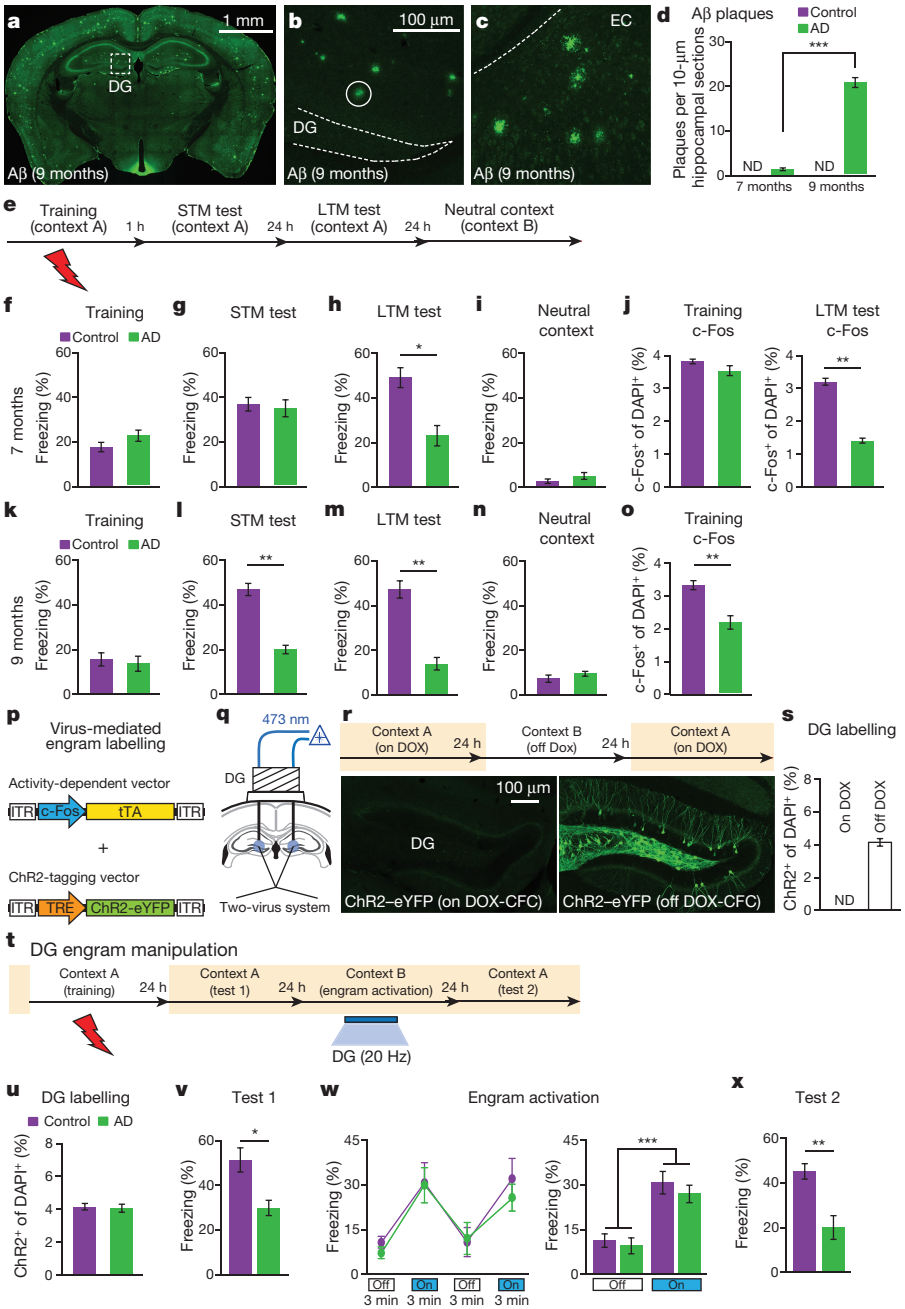

Figure 1 | Optogenetic activation of memory engrams restores fear memory in early AD mice. a–c, Amyloid-β (Aβ) plaques in 9-month-old AD mice (**a**), in the DG (**b**), and in the EC (**c**). **d**, Plaque counts in HPC sections ($n = 4$ mice per group). ND, not detected. **e**, CFC behavioural schedule ($n = 10$ mice per group). **f–i**, Freezing levels of 7-month-old AD groups during training (**f**), STM test (**g**), LTM test (**h**) or exposure to neutral context (**i**). **j**, c-Fos$^+$ cell counts in the DG of 7-month-old mice after CFC training or LTM test, represented in **f**, **h** ($n = 4$ mice per group). DAPI, 4′,6-diamidino-2-phenylindole. **k–n**, Freezing levels of 9-month-old AD mice during training (**k**), STM test (**l**), LTM test (**m**) or exposure to neutral context (**n**). **o**, c-Fos$^+$ cell counts in the DG of 9-month-old mice ($n = 3$ mice per group) after CFC training represented in **k**. **p**, Virus-mediated engram labelling strategy using a cocktail of AAV$_9$-c-Fos-tTA and AAV$_9$-TRE-ChR2-eYFP. **q**, AD mice were injected with the two viruses bilaterally and implanted with an optic fibre bilaterally into the DG. **r**, Behavioural schedule and DG engram cell labelling (see Methods). **s**, ChR2–eYFP$^+$ cell counts from DG sections shown in **r** ($n = 3$ mice per group). **t**, Behavioural schedule for optogenetic activation of DG engram cells. **u**, ChR2–eYFP$^+$ cell counts from 7-month-old mice ($n = 5$ mice per group). **v**, Memory recall in context A 1 day after training (test 1, $n = 9$ mice per group). **w**, Freezing by blue light stimulation (left). Average freezing for two light-off and light-on epochs (right). **x**, Memory recall in context A 3 days after training (test 2). Statistical comparisons are performed using unpaired *t*-tests; $^*P < 0.05$, $^{**}P < 0.01$, $^{***}P < 0.001$. Data are presented as mean ± standard error of the mean (s.e.m.).

Reduced dendritic spines have been implicated in memory impairments of AD[3]. In addition, our recent study of protein-synthesis-inhibitor-induced amnesia found reduced engram-cell-specific dendritic spine density[14]. We detected an age-dependent (Extended Data Fig. 5a) decrease in dendritic spine density of DG engram cells in early AD mice (Fig. 2a–c), showing that the long-term memory impairments of early AD correlate with dendritic spine deficits of DG engram cells (Extended Data Fig. 5b). The inability to generate newborn neurons in the DG could play a part in the development of AD-specific cognitive deficits[19]. However, early AD mice showed similar levels of neurogenesis in the DG compared with control mice, which were quantified using doublecortin (DCX) staining (Extended Data Fig. 1l–q). We recently proposed that the persistent cellular connectivity between multiple engram cell ensembles is a fundamental mechanism of memory information

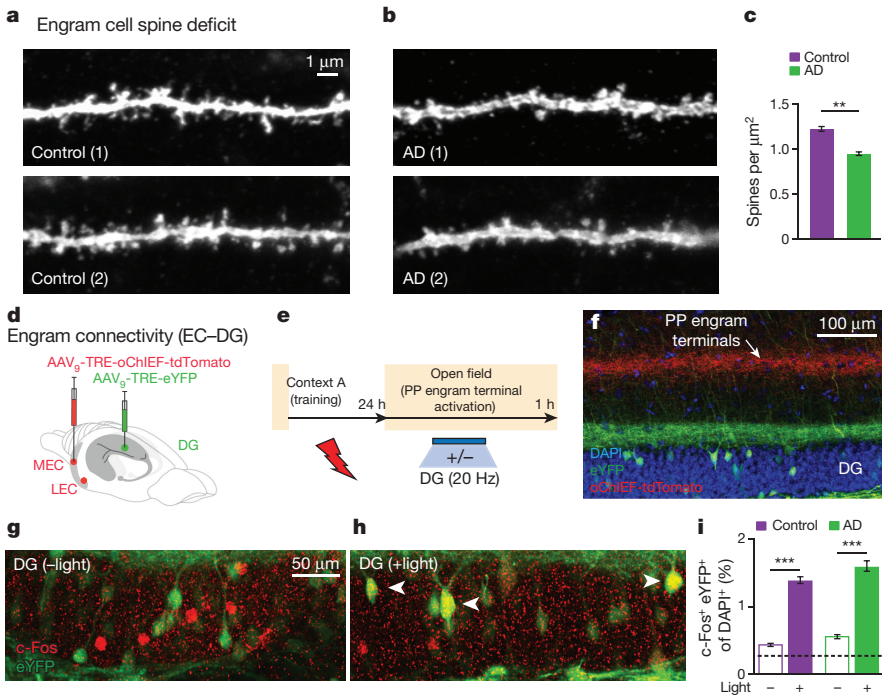

Figure 2 | Neural correlates of amnesia in early AD mice. **a**, **b**, Images showing dendritic spines from DG engram cells of control (**a**) and AD (**b**) groups. **c**, Average spine density showing a decrease in AD mice ($n = 7{,}032$ spines) compared with controls ($n = 9{,}437$ spines, $n = 4$ mice per group). **d**, For engram connectivity, MEC/LEC and DG cells were injected with virus cocktails. **e**, Engram connectivity behavioural schedule. Mice ($n = 4$ per group) were either given a natural exploration session (−) or a PP engram terminal stimulation session (+) in an open field. **f**, Image showing simultaneous labelling of engram terminals (red) and engram cells (green). Green terminals reflect mossy cell axons. **g**, **h**, Images showing c-Fos$^+$/eYFP$^+$ overlap in the DG. **i**, c-Fos$^+$/eYFP$^+$ counts from control and AD mice. Chance overlap (0.24) was calculated (see Methods) and indicated by the dashed line. Statistical comparisons are performed using unpaired *t*-tests; $^{**}P < 0.01$, $^{***}P < 0.001$. Data are presented as mean ± s.e.m.

retention[14]. We labelled putative CFC memory engram cells in both medial EC (MEC) and lateral EC (LEC) with oChIEF[20] (a variant of ChR2) and simultaneously labelled CFC memory engram cells in the DG with eYFP (Fig. 2d). With this procedure, perforant path (PP) terminals are also labelled with oChIEF (Fig. 2e, f). One day after foot-shocks, we optogenetically activated these terminals and quantified the overlap between putative DG engram cells (that is, eYFP$^+$, green) and DG cells in which the endogenous c-Fos (red) had been activated by the optogenetic activation of oChIEF$^+$ PP terminals. Both control and early AD mice showed above-chance and indistinguishable levels of c-Fos$^+$/eYFP$^+$ overlap, indicating that the preferential functional connectivity between engram cells is maintained in the early AD mice (Fig. 2g–i).

We then hypothesized that the reversal of dendritic spine deficits in DG engram cells of early AD mice may rescue long-term memory. To investigate this possibility, we took advantage of previous findings that spine formation can be induced rapidly by long-term potentiation (LTP)[21,22] and that LTP can be induced *in vivo* using light activation of oChIEF[23]. We validated learning-dependent labelling, with oChIEF, of neurons in the MEC (Fig. 3a–c and Extended Data Fig. 6a–c) and LEC (Fig. 3d) as well as PP terminals in the DG (Fig. 3e, f). *In vivo* extracellular recording upon light stimulation of oChIEF$^+$ EC axonal terminals in the DG showed a reliable spiking response of DG cells in anaesthetized control mice (Fig. 3g). Furthermore, in HPC slices from control mice we successfully induced LTP in DG cells using a previously established optical LTP protocol[23] (Fig. 3h–j). These biocytin-filled DG cells revealed an increase in spine density after *in vitro* optical LTP (Extended Data Fig. 6d).

In early AD mice, *in vivo* application of the engram-specific optical LTP protocol restored spine density of DG engram cells to control levels (AD + 100 Hz group; Fig. 3k, l). Furthermore, this spine restoration in early AD mice correlated with amelioration of long-term memory impairments observed during recall by natural cues (Fig. 3m), an effect that persisted for at least 6 days after training (AD rescue + diphtheria toxin receptor (DTR) + saline group; Fig. 3p). The LTP-induced spine restoration and behavioural deficit rescue were protein-synthesis dependent (Extended Data Fig. 7). The rescued memory was context-specific (Extended Data Fig. 8a). In addition, long-term memory recall of age-matched control mice was unaffected by this optical LTP protocol (Extended Data Fig. 8b). By contrast, applying the optical LTP protocol to a large portion of excitatory PP terminals in the DG (that is, with no restriction to the PP terminals derived from EC engram cells) did not result in long-term memory rescue in early AD mice (Extended Data Fig. 9). To confirm the correlation between restoration of spine density of DG engram cells and amelioration of long-term memory impairments, which were both induced by the optical LTP protocol, we compared the overlap of natural-recall-cue-induced c-Fos$^+$ cells and CFC-training-labelled DG engram cells after an application of the engram-specific LTP protocol to early AD mice (Fig. 3n). Early AD mice that did not receive the optical LTP protocol showed low levels of c-Fos$^+$/eYFP$^+$ overlap compared with control mice upon natural recall cue delivery. By contrast, early AD mice that went through the optical LTP protocol showed c-Fos$^+$/eYFP$^+$ overlap similar to that of control mice (Fig. 3n). Thus, these data suggest that spine density restoration in DG engram cells contributes to the rescue of long-term memory in early AD mice.

Because of the highly redundant connectivity between the EC and DG[24], it is possible that the extensive optical LTP protocol also augmented spine density in some non-engram DG cells. To establish a link between the spine rescue in DG engram cells and the behavioural rescue of early AD mice, we developed an engram-specific ablation[25] virus. We confirmed that this DTR-mediated method efficiently ablated DG engram cells after diphtheria toxin (DT) administration (Fig. 3o), while leaving the nearby DG mossy cells intact (Extended Data Fig. 10). By simultaneously labelling axonal terminals of PP with oChIEF and DG engram cells with DTR, we examined the effect of DG engram cell ablation after optical LTP-induced behavioural rescue (Fig. 3p). Within-animal comparisons (test 1 versus test 2) showed a decrease in freezing behaviour of LTP-rescued AD mice in which DG engram cells were ablated. These data strengthen the link between DG engram cells with restored spine density and long-term behavioural rescue in early AD mice.

To examine whether the optical LTP-induced behavioural rescue could be applied to DG engram cells from other learning experiences, we labelled memory engrams for inhibitory avoidance or novel object location in early AD mice (Fig. 4a). Early AD mice showed memory impairments in inhibitory avoidance memory and novel object location spatial memory (Fig. 4b, c). Optical LTP-induced spine rescue at the PP–DG engram synapses was sufficient to reverse long-term memory impairments of early AD mice in both behavioural paradigms, thus demonstrating the versatility of our engram-based intervention.

Previous studies that examined the early stages of AD found correlations between memory impairments and synaptic pathology at the

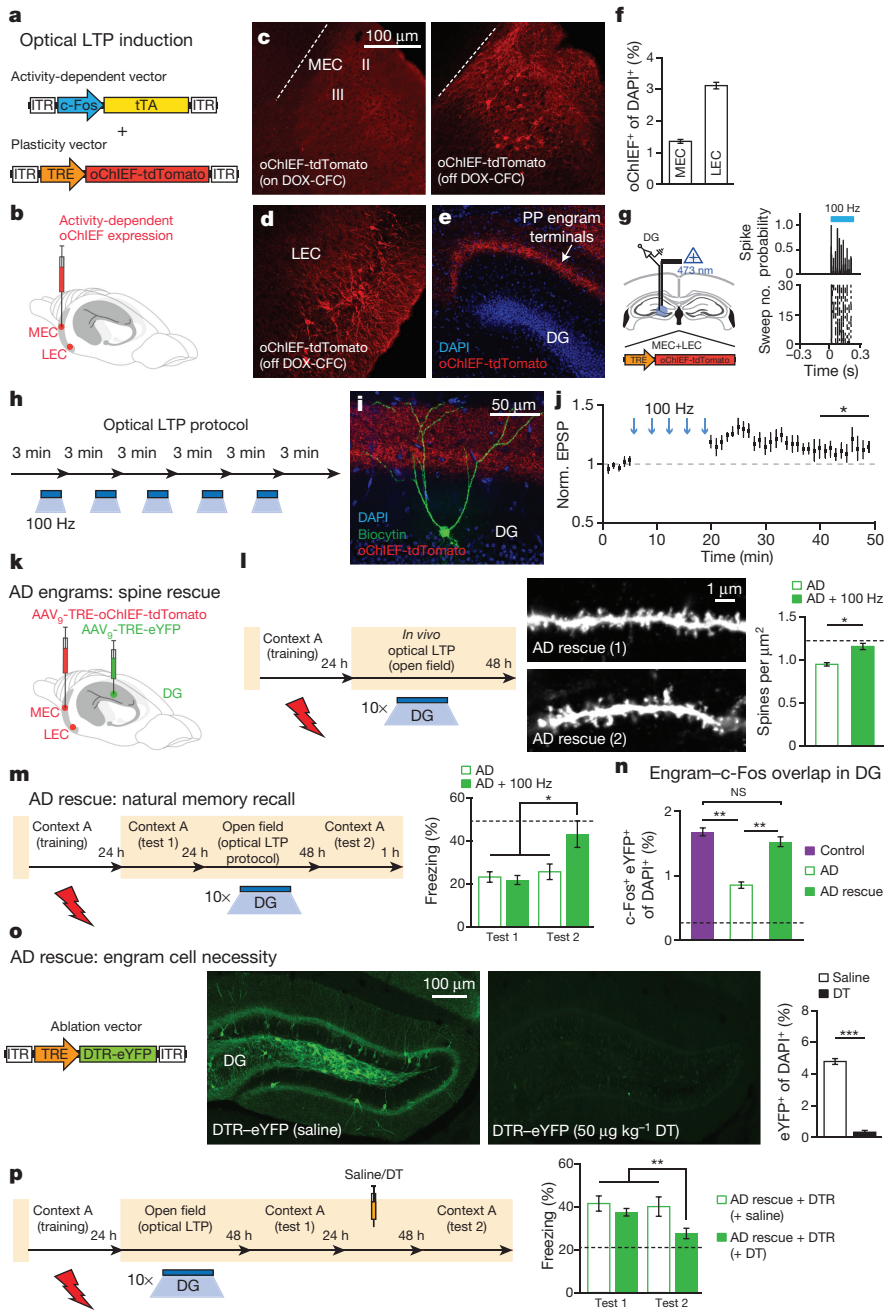

Figure 3 | Reversal of engram-specific spine deficits rescues memory in early AD mice. **a**, Engram-specific optical LTP using two viruses. **b**, Virus cocktail injected into MEC/LEC. **c–e**, Images showing oChIEF labelling 24 h after CFC: in MEC on DOX (left; **c**) and off DOX (right; **c**); in LEC off DOX (**d**); in DG off DOX (sagittal; **e**). Scale bar shown in **c** applies to **d** and **e**. **f**, oChIEF$^+$ cell counts ($n = 3$ mice per group). **g**, *In vivo* spiking of DG neurons in response to 100 Hz light applied to PP terminals. **h**, Optical LTP protocol[23]. **i**, **j**, *In vitro* responses of DG cells after optical LTP. Image showing biocytin-filled DG cell receiving oChIEF$^+$ PP terminals (coronal; **i**). Normalized (Norm.) excitatory post-synaptic potentials (EPSPs) showing a 10% increase in amplitude ($n = 6$ cells; **j** and Methods). **k**, For *in vivo* optical LTP at EC–DG synapses, MEC/LEC and DG cells were injected with virus cocktails. **l**, Protocol for *in vivo* spine restoration of DG engram cells in AD mice (left). Images showing dendritic spines of DG engram cells after LTP (middle). A two-way analysis of variance (ANOVA) followed by Bonferroni post-hoc tests revealed a spine density restoration in AD + 100 Hz mice ($F_{1,211} = 7.21$, $P < 0.01$, 13,025 spines, $n = 4$ mice per group; right). Dashed line represents control mice spine density (1.21). **m**, Behavioural schedule for memory rescue in AD mice (left). A two-way ANOVA with repeated measures followed by Bonferroni post-hoc tests revealed restored freezing in AD + 100 Hz mice ($F_{1,36} = 4.95$, $P < 0.05$, $n = 10$ mice per group; right). Dashed line represents control mice freezing (48.53). **n**, After rescue, mice were perfused for c-Fos$^+$/eYFP$^+$ overlap cell counts. Chance was estimated at 0.22. NS, not significant. **o**, Construct for ablation of engram cells using DTR (left). Images showing DG engram cells after saline/DT administration (middle). DTR–eYFP cell counts ($n = 5$ mice per group; right). **p**, Behavioural schedule testing the necessity of engram cells after spine restoration (left). Memory recall showed less freezing of AD mice treated with DT (AD rescue + DTR + DT) compared with saline-treated mice ($n = 9$ mice per group; right). Dashed line represents freezing of non-stimulated early AD mice (20.48). Unless specified, statistical comparisons are performed using unpaired *t*-tests; $^*P < 0.05$, $^{**}P < 0.01$, $^{***}P < 0.001$. Data are presented as mean ± s.e.m.

EC PP input into the DG[3,4,6]. It has been proposed that these early cognitive deficits are a failure of memory encoding on the basis of behavioural observations in human patients[8,9]. However, we have shown that optogenetic activation of HPC cells active during learning elicits memory recall in mouse models of early AD. To our knowledge, this is the first rigorous demonstration that memory failure in early AD models reflects an impairment in the retrieval of information. Further support for a memory retrieval impairment in early AD comes from the fact that impairments are in LTM (at least 1 day long), but not in STM (~1 h after training), which is consistent with a retrieval deficit. The retrieval deficit in early AD models is similar to memory deficits observed in amnesia induced by impairing memory consolidation via protein synthesis inhibitors[14]. The underlying mechanism of memory failure in early AD patients may not necessarily parallel the molecular and circuit impairments observed in mouse models of early AD. For instance, some early AD patients can exhibit amyloid plaque deposition years before the onset of cognitive decline[9]. However, converging data on the underlying mechanism for genetically and pharmacologically induced amnesia in animal models increase the possibility that similar memory-retrieval-based failures may also operate in an early stage of AD patients. While we have shown that amnesia in early AD mice is a deficit of memory retrieval, it remains possible that the long-term maintenance of memory storage may also gradually become compromised as the disease proceeds from the early stage to more advanced stages, and eventually lost with neuronal degeneration. Further research will investigate these possibilities.

Our conclusions apply to episodic memory, which involves processing by HPC and other medial temporal lobe structures. In the literature[9], it is widely recognized that early AD patients exhibit non-episodic memory deficits as well, which would involve brain structures other than the medial temporal lobe. Additional work is required to examine the mechanisms underlying cognitive impairments in these other types of memories. Nevertheless, our findings already contribute to a better understanding of memory retrieval deficits in several cases of early AD, and may apply to other pathological conditions, such as Huntington's disease[8], in which patients show difficulty in memory recall.

Consistent with several studies highlighting the importance of dendritic spines[3,6,14,26] in relation to memory processing, we observed an engram-cell-specific decrease in spine density that correlated with

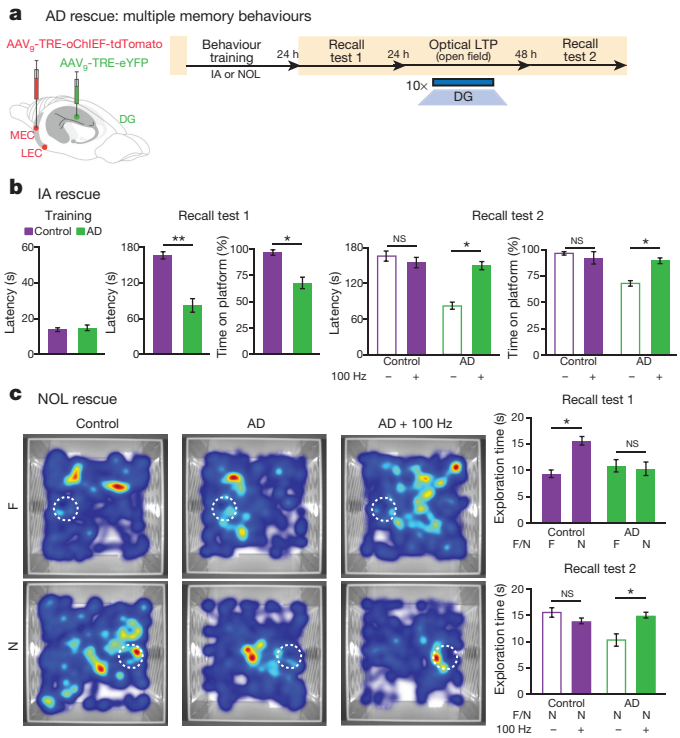

Figure 4 | Recovery of multiple types of HPC-dependent memories from amnesia in early AD. a, MEC/LEC and DG cells were injected with virus cocktails (left). Behavioural schedule for engram labelling (right). **b**, Inhibitory avoidance (IA) long-term rescue ($n = 10$ mice per group). Recall test 1 showed decreased latency and time on platform for AD mice. A two-way ANOVA with repeated measures followed by Bonferroni post-hoc tests revealed a recovery of IA memory in early AD mice (latency: $F_{1,27} = 25.22$, $P < 0.001$; time on platform: $F_{1,27} = 6.46$, $P < 0.05$; recall test 2). **c**, Novel object location (NOL) long-term rescue ($n = 15$ mice per group). Average heat maps showing exploration time for familiar (F) or novel (N) locations (left or right, respectively). White circles represent object location. Recall test 1 showed comparable exploration of familiar locations by control and AD mice; however, AD mice showed decreased exploration of novel locations. A two-way ANOVA with repeated measures followed by Bonferroni post-hoc tests revealed a recovery of NOL memory in early AD mice ($F_{1,56} = 5.87$, $P < 0.05$; recall test 2). Unless specified, statistical comparisons are performed using unpaired *t*-tests; $^{*}P < 0.05$, $^{**}P < 0.01$. Data are presented as mean ± s.e.m. NS, not significant.

memory deficits in early AD. Natural rescue of memory recall in early AD mice required the DG engram cells in which synaptic density deficits have been restored by *in vivo* optical LTP protocols applied to the EC cells activated during learning. By contrast, the application of optical LTP protocols to a much wider array of excitatory EC cells projecting to the DG, which may be analogous to deep brain stimulation, did not rescue memory in AD mice. A potential explanation for this observation is that DG granule cells may contribute to a variety of memories through their partially overlapping engram cell ensembles in a competitive manner, and that activation of a large number of these ensembles simultaneously may interfere with a selective activation of an individual ensemble. Thus, activation of a more targeted engram cell ensemble may be a key requirement for effective retrieval of the specific memory, which is difficult to achieve with the current deep brain stimulation strategy.

Genetic manipulations of specific neuronal populations can have profound effects on cognitive impairments of AD[27]. We propose that strategies applied to engram circuits can support long-lasting improvements in cognitive functions, which may provide insights and therapeutic value for future approaches that rescue memory in AD patients.

Online Content Methods, along with any additional Extended Data display items and Source Data, are available in the online version of the paper; references unique to these sections appear only in the online paper.

Received 6 August 2015; accepted 28 January 2016.
Published online 16 March 2016.

1. Selkoe, D. J. Alzheimer's disease: genes, proteins, and therapy. *Physiol. Rev.* **81,** 741–766 (2001).
2. Selkoe, D. J. Alzheimer's disease is a synaptic failure. *Science* **298,** 789–791 (2002).
3. Jacobsen, J. S. *et al.* Early-onset behavioral and synaptic deficits in a mouse model of Alzheimer's disease. *Proc. Natl Acad. Sci. USA* **103,** 5161–5166 (2006).
4. Hsia, A. Y. *et al.* Plaque-independent disruption of neural circuits in Alzheimer's disease mouse models. *Proc. Natl Acad. Sci. USA* **96,** 3228–3233 (1999).
5. Mucke, L. *et al.* High-level neuronal expression of $A\beta_{1-42}$ in wild-type human amyloid protein precursor transgenic mice: synaptotoxicity without plaque formation. *J. Neurosci.* **20,** 4050–4058 (2000).
6. Terry, R. D. *et al.* Physical basis of cognitive alterations in Alzheimer's disease: synapse loss is the major correlate of cognitive impairment. *Ann. Neurol.* **30,** 572–580 (1991).
7. Granholm, E. & Butters, N. Associative encoding and retrieval in Alzheimer's and Huntington's disease. *Brain Cogn.* **7,** 335–347 (1988).
8. Hodges, J. R., Salmon, D. P. & Butters, N. Differential impairment of semantic and episodic memory in Alzheimer's and Huntington's diseases: a controlled prospective study. *J. Neurol. Neurosurg. Psychiatry* **53,** 1089–1095 (1990).
9. Weintraub, S., Wicklund, A. H. & Salmon, D. P. The neuropsychological profile of Alzheimer disease. *Cold Spring Harb. Perspect. Med.* **2,** a006171 (2012).
10. Jankowsky, J. L. *et al.* Mutant presenilins specifically elevate the levels of the 42 residue β-amyloid peptide *in vivo*: evidence for augmentation of a 42-specific γ secretase. *Hum. Mol. Genet.* **13,** 159–170 (2004).
11. Liu, X. *et al.* Optogenetic stimulation of a hippocampal engram activates fear memory recall. *Nature* **484,** 381–385 (2012).
12. Ramirez, S. *et al.* Creating a false memory in the hippocampus. *Science* **341,** 387–391 (2013).
13. Redondo, R. L. *et al.* Bidirectional switch of the valence associated with a hippocampal contextual memory engram. *Nature* **513,** 426–430 (2014).
14. Ryan, T. J., Roy, D. S., Pignatelli, M., Arons, A. & Tonegawa, S. Engram cells retain memory under retrograde amnesia. *Science* **348,** 1007–1013 (2015).
15. Denny, C. A. *et al.* Hippocampal memory traces are differentially modulated by experience, time, and adult neurogenesis. *Neuron* **83,** 189–201 (2014).
16. Harris, J. A. *et al.* Transsynaptic progression of amyloid-β-induced neuronal dysfunction within the entorhinal-hippocampal network. *Neuron* **68,** 428–441 (2010).
17. Hyman, B. T., Van Hoesen, G. W., Kromer, L. J. & Damasio, A. R. Perforant pathway changes and the memory impairment of Alzheimer's disease. *Ann. Neurol.* **20,** 472–481 (1986).
18. Oddo, S. *et al.* Triple-transgenic model of Alzheimer's disease with plaques and tangles: intracellular Aβ and synaptic dysfunction. *Neuron* **39,** 409–421 (2003).
19. Rodríguez, J. J. *et al.* Impaired adult neurogenesis in the dentate gyrus of a triple transgenic mouse model of Alzheimer's disease. *PLoS One* **3,** e2935 (2008).
20. Lin, J. Y., Lin, M. Z., Steinbach, P. & Tsien, R. Y. Characterization of engineered channelrhodopsin variants with improved properties and kinetics. *Biophys. J.* **96,** 1803–1814 (2009).
21. Maletic-Savatic, M., Malinow, R. & Svoboda, K. Rapid dendritic morphogenesis in CA1 hippocampal dendrites induced by synaptic activity. *Science* **283,** 1923–1927 (1999).
22. Engert, F. & Bonhoeffer, T. Dendritic spine changes associated with hippocampal long-term synaptic plasticity. *Nature* **399,** 66–70 (1999).
23. Nabavi, S. *et al.* Engineering a memory with LTD and LTP. *Nature* **511,** 348–352 (2014).
24. Tamamaki, N. & Nojyo, Y. Projection of the entorhinal layer II neurons in the rat as revealed by intracellular pressure-injection of neurobiotin. *Hippocampus* **3,** 471–480 (1993).
25. Zhan, C. *et al.* Acute and long-term suppression of feeding behavior by POMC neurons in the brainstem and hypothalamus, respectively. *J. Neurosci.* **33,** 3624–3632 (2013).
26. Tonegawa, S., Liu, X., Ramirez, S. & Redondo, R. Memory engram cells have come of age. *Neuron* **87,** 918–931 (2015).
27. Cissé, M. *et al.* Reversing EphB2 depletion rescues cognitive functions in Alzheimer model. *Nature* **469,** 47–52 (2011).

Acknowledgements We thank X. Liu for the c-Fos-tTA construct; S. Huang, T. Okuyama and T. Kitamura for help with experiments; W. Yu, S. LeBlanc and X. Zhou for technical assistance; L. Brenner for proofreading; and all members of the Tonegawa laboratory for their support. We thank M. Luo for sharing the DTR coding sequence. This work was supported by the RIKEN Brain Science Institute, the Howard Hughes Medical Institute, and the JPB Foundation (to S.T.).

Author Contributions D.S.R. and S.T. contributed to the study design. D.S.R., A.A., T.I.M., M.P. and T.J.R. contributed to the data collection and interpretation. D.S.R. cloned all constructs. D.S.R. and A.A. conducted the surgeries, behaviour experiments and histological analyses. D.S.R. and S.T. wrote the paper. All authors discussed and commented on the manuscript.

Author Information Reprints and permissions information is available at www.nature.com/reprints. The authors declare no competing financial interests. Readers are welcome to comment on the online version of the paper. Correspondence and requests for materials should be addressed to S.T. (tonegawa@mit.edu).

METHODS

Subjects. The APP/PS1 (ref. 10) double-transgenic AD mice, originally described as Line 85, were obtained from Jackson Laboratory (stock number 004462). Under the control of mouse prion promoter elements, these mice express a chimaeric mouse/human *APP* transgene containing Swedish mutations (K595N/M596L) as well as a mutant human *PS1* transgene (delta exon 9 variant). To label memory engram cells in APP/PS1 mice, we generated a triple-transgenic mouse line by mating *c-Fos-tTA*[11,28] transgenic mice with APP/PS1 double-transgenic mice. The PS1/APP/tau[18] triple-transgenic AD mice were obtained from Jackson Laboratory (stock number 004807). These 3×Tg-AD mice express a mutant human *PS1* transgene (M146V), a human *APP* transgene containing Swedish mutations (KM670/671NL) and a human *MAPT* transgene harbouring the P301L mutation. All mouse lines were maintained as hemizygotes. Mice had access to food and water *ad libitum* and were socially housed in numbers of two to five littermates until surgery. After surgery, mice were singly housed. For behavioural experiments, all mice were male and 7–9 months old. For optogenetic experiments, mice had been raised on food containing 40 mg kg^{-1} DOX for at least 1 week before surgery, and remained on DOX for the remainder of the experiments except for the target engram labelling days. For *in vitro* electrophysiology experiments, mice were 24–28 days old at the time of surgery. All experiments were conducted in accordance with US National Institutes of Health (NIH) guidelines and the Massachusetts Institute of Technology Department of Comparative Medicine and Committee of Animal Care. No statistical methods were used to predetermine sample size.

Viral constructs. Our previously established method[11] for labelling memory engram cells combined c-Fos-tTA transgenic mice with a DOX-sensitive adeno-associated virus (AAV). However, in this study, we modified the method using a double-virus system to label memory engram cells in the early AD mice, which already carry two transgenes. The pAAV-c-Fos-tTA plasmid was constructed by cloning a 1 kb fragment from the *c-Fos* gene (550 bp upstream of *c-Fos* exon I to 35 bp into exon II) into an AAV backbone using the KpnI restriction site at the 5′ terminus and the SpeI restriction site at the 3′ terminus. The AAV backbone contained the tTA-Advanced[29] sequence at the SpeI restriction site. The pAAV-TRE-ChR2-eYFP and pAAV-TRE-eYFP constructs were previously described[11,12]. The pAAV-TRE-oChIEF-tdTomato[20] plasmid was constructed by replacing the ChR2-eYFP fragment from the pAAV-TRE-ChR2-eYFP plasmid using NheI and MfeI restriction sites. The pAAV-CaMKII-oChIEF-tdTomato plasmid was constructed by replacing the TRE fragment from the pAAV-TRE-oChIEF-tdTomato plasmid using BamHI and EcoRI restriction sites. The pAAV-TRE-DTR-eYFP[25] plasmid was constructed by replacing the ChR2 fragment from the pAAV-TRE-ChR2-eYFP plasmid using EcoRI and AgeI restriction sites. AAV vectors were serotyped with AAV_9 coat proteins and packaged at the University of Massachusetts Medical School Gene Therapy Center and Vector Core. Viral titres were 1.5×10^{13} genome copy (GC) ml^{-1} for AAV_9-c-Fos-tTA, AAV_9-TRE-ChR2-eYFP and AAV_9-TRE-eYFP, 1×10^{13} GC ml^{-1} for AAV_9-TRE-oChIEF-tdTomato, 4×10^{13} GC ml^{-1} for AAV_9-CaMKII-oChIEF-tdTomato and 2×10^{13} GC ml^{-1} for AAV_9-TRE-DTR-eYFP.

Surgery and optic fibre implants. Mice were anaesthetized with isoflurane or 500 mg kg^{-1} avertin for stereotaxic injections[14]. Injections were targeted bilaterally to the DG (−2.0 mm anteroposterior (AP), ±1.3 mm mediolateral (ML), −1.9 mm dorsoventral (DV)), MEC (−4.7 mm AP, ±3.35 mm ML, −3.3 mm DV) and LEC (−3.4 mm AP, ±4.3 mm ML, −4.0 mm DV). Injection volumes were 300 nl for DG and 400 nl for MEC and LEC. Viruses were injected at 70 nl min^{-1} using a glass micropipette attached to a 10 ml Hamilton microsyringe. The needle was lowered to the target site and remained for 5 min before beginning the injection. After the injection, the needle stayed for 10 min before it was withdrawn. A custom DG implant containing two optic fibres (200 mm core diameter; Doric Lenses) was lowered above the injection site (−2.0 mm AP, ±1.3 mm ML, −1.7 mm DV). The implant was secured to the skull with two jewellery screws, adhesive cement (C&B Metabond) and dental cement. An opaque cap derived from the top part of an Eppendorf tube protected the implant. Mice were given 1.5 mg kg^{-1} metacam as analgesic and allowed to recover for 2 weeks before behavioural experiments. All injection sites were verified histologically. As criteria, we only included mice with virus expression limited to the targeted regions.

Systemic injection of kainic acid. For seizure experiments[11], mice were taken off DOX for 1 day and injected intraperitoneally with 15 mg kg^{-1} kainic acid (KA). Mice were returned to DOX food 6 h after KA treatment and perfused the next day for immunohistochemistry procedures.

Immunohistochemistry. Mice were dispatched using 750–1,000 mg kg^{-1} avertin and perfused transcardially with PBS, followed by 4% paraformaldehyde (PFA). Brains were extracted and incubated in 4% PFA at room temperature overnight. Brains were transferred to PBS and 50-μm coronal slices were prepared using a vibratome. For immunostaining[14], each slice was placed in PBS + 0.2% Triton X-100 (PBS-T), with 5% normal goat serum for 1 h and then incubated with primary antibody at 4 °C for 24 h. Slices then underwent three wash steps for 10 min each in PBS-T, followed by 1 h incubation with secondary antibody. After three more wash steps of 10 min each in PBS-T, slices were mounted on microscope slides. All analyses were performed blind to the experimental conditions. Antibodies used for staining were as follows: to stain for ChR2–eYFP, DTR–eYFP or eYFP alone, slices were incubated with primary chicken anti-GFP (1:1,000, Life Technologies) and visualized using anti-chicken Alexa-488 (1:200). For plaques, slices were stained using primary mouse anti-β-amyloid (1:1,000; Sigma-Aldrich) and secondary anti-mouse Alexa-488 (1:500). c-Fos was stained with rabbit anti-c-Fos (1:500, Calbiochem) and anti-rabbit Alexa-568 (1:300). Adult newborn neurons were stained with guinea pig anti-DCX (1:1,000; Millipore) and anti-guinea-pig Alexa-555 (1:500). Neuronal nuclei were stained with mouse anti-NeuN (1:200; Millipore) and Alexa-488 (1:200). DG mossy cell axons were stained with mouse anti-CR (1:1,000; Swant) and Alexa-555 (1:300).

Cell counting. To characterize the expression pattern of ChR2–eYFP, DTR–eYFP, eYFP alone and oChIEF-tdTomato in control and AD mice, the number of eYFP$^+$/tdTomato$^+$ neurons were counted from 4–5 coronal slices per mouse ($n = 3$–5 mice per group). Coronal slices centred on coordinates covered by optic fibre implants were taken for DG quantification and sagittal slices centred on injection coordinates were taken for MEC and LEC. Fluorescence images were acquired using a Zeiss AxioImager.Z1/ApoTome microscope (×20). Automated cell counting analysis was performed using ImageJ software. The cell body layers of DG granule cells (upper blade), MEC or LEC cells were outlined as a region of interest (ROI) according to the DAPI signal in each slice. The number of eYFP$^+$/tdTomato$^+$ cells per section was calculated by applying a threshold above background fluorescence. Data were analysed using Microsoft Excel with the Statplus plug-in. A similar approach was applied for quantifying amyloid-β plaques, c-Fos$^+$ neurons and adult newborn (DCX$^+$) neurons. Total engram cell reactivation was calculated as ((c-Fos$^+$ eYFP$^+$)/(total DAPI$^+$)) × 100. Chance overlap was calculated as ((c-Fos$^+$/total DAPI$^+$) × (eYFP$^+$/total DAPI$^+$)) × 100. Percentage of adult newborn neurons expressing neuronal markers was calculated as ((NeuN$^+$ DCX$^+$)/(total DCX$^+$) × 100. DAPI$^+$ counts were approximated from five coronal/sagittal slices using ImageJ. All counting experiments were conducted blind to experimental group. Researcher 1 trained the animals, prepared slices and randomized images, while researcher 2 performed semi-automated cell counting. Statistical comparisons were performed using unpaired *t*-tests: $*P < 0.05$, $**P < 0.01$, $***P < 0.001$.

Spine density analysis. Engram cells were labelled using c-Fos-tTA-driven synthesis of ChR2–eYFP or eYFP alone. The eYFP signal was amplified using immunohistochemistry procedures, after which fluorescence *z*-stacks were taken by confocal microscopy (Zeiss LSM700) using a ×40 objective. Maximum intensity projections were generated using ZEN Black software (Zeiss). Four mice per experimental group were analysed for dendritic spines. For each mouse, 30–40 dendritic fragments of 10-μm length were quantified ($n = 120$–160 fragments per group). To measure spine density of DG engram cells with a focus on entorhinal cortical inputs, distal dendritic fragments in the middle-to-outer molecular layer (ML) were selected. For CA3 and CA1 engram cells, apical and basal dendritic fragments were selected. To compute spine density, the number of spines counted on each fragment was normalized by the cylindrical approximation of the surface of the specific fragment. Experiments were conducted blind to experimental group. Researcher 1 imaged dendritic fragments and randomized images, while researcher 2 performed manual spine counting.

***In vitro* recordings.** After isoflurane anaesthesia, brains were quickly removed and used to prepare sagittal slices (300 μm) in an oxygenated cutting solution at 4 °C with a vibratome[14]. Slices were incubated at room temperature in oxygenated artificial cerebrospinal fluid (ACSF) until the recordings. The cutting solution contained (in mM): 3 KCl, 0.5 $CaCl_2$, 10 $MgCl_2$, 25 $NaHCO_3$, 1.2 NaH_2PO_4, 10 D-glucose, 230 sucrose, saturated with 95% O_2–5% CO_2 (pH 7.3, osmolarity of 340 mOsm). The ACSF contained (in mM): 124 NaCl, 3 KCl, 2 $CaCl_2$, 1.3 $MgSO_4$, 25 $NaHCO_3$, 1.2 NaH_2PO_4, 10 D-glucose, saturated with 95% O_2–5% CO_2 (pH 7.3, 300 mOsm). Individual slices were transferred to a submerged experimental chamber and perfused with oxygenated ACSF warmed at 35 °C (±0.5 °C) at a rate of 3 ml min^{-1} during recordings. Current or voltage clamp recordings were performed under an IR-DIC microscope (Olympus) with a ×40 water immersion objective (0.8 NA), equipped with four automatic manipulators (Luigs & Neumann) and a CCD camera (Hamamatsu). Borosilicate glass pipettes (Sutter Instruments) were fabricated with resistances of 8–10 MΩ. The intracellular solution (in mM) for current clamp recordings was: 110 K-gluconate, 10 KCl, 10 HEPES, 4 ATP, 0.3 GTP, 10 phosphocreatine, 0.5% biocytin (pH 7.25, 290 mOsm). Recordings used two dual channel amplifiers (Molecular Devices), a 2 kHz filter, 20 kHz digitization and an ADC/DAC

data acquisition unit (Instrutech) running on custom software in Igor Pro (Wavemetrics). Data acquisition was suspended whenever the resting membrane potential was depolarized above −50 mV or the access resistance (RA) exceeded 20 MΩ. Optogenetic stimulation was achieved using a 460 nm LED light source (Lumen Dynamics) driven by TTL input with a delay onset of 25 μs (subtracted offline for latency estimation). Light power on the sample was 33 mW mm^{-2}. To test oChIEF expression, EC cells were stimulated with a single light pulse of 1 s, repeated 10 times every 5 s. DG granule cells were held at −70 mV. Optical LTP protocol: 5 min baseline (10 blue light pulses of 2 ms each, repeated every 30 s) was acquired before the onset of the LTP protocol (100 blue light pulses of 2 ms each at a frequency of 100 Hz, repeated 5 times every 3 min) and the effect on synaptic amplitude was recorded for 30 min (1 pulse of 2 ms every 30 s). Using the 5 min baseline recording data, EPSPs were normalized (Fig. 3j). Potentiation was observed in 6 out of 30 cells and results were statistically confirmed using a two-tailed paired *t*-test. Experiments were performed in the presence of 10 μM gabazine (Tocris) and 2 μM CGP55845 (Tocris). Recorded cells were recovered for morphological identification using streptavidin CF633 (Biotium).

***In vivo* recordings.** Multi-unit responses to optical stimulation were recorded in the DG of mice injected with a cocktail of AAV_9-c-Fos-tTA and AAV_9-TRE-oChIEF-tdTomato viruses into MEC/LEC. Mice were anaesthetized (10 ml kg^{-1}) using a mixture of ketamine (100 mg ml^{-1})/xylazine (20 mg ml^{-1}) and placed in the stereotactic system. Anaesthesia was maintained by booster doses of ketamine (100 mg kg^{-1}). An optrode consisting of a tungsten electrode (0.5 MΩ) attached to an optic fibre (200-μm core diameter), with the tip of the electrode extending beyond the tip of the fibre by 300 μm, was used for simultaneous optical stimulation and extracellular recording. The power intensity of light emitted from the optrode was calibrated to about 10 mW, consistent with the power used in behavioural assays. oChIEF$^+$ cells were identified by delivering 20-ms light pulses (1 Hz) to the recording site every 50–100 μm. After light-responsive cells were detected, multi-unit activity in response to trains of light pulses (200 ms) at 100 Hz was recorded. Data acquisition used an Axon CNS Digidata 1440A system. MATLAB analysis was performed, as previously described[12].

Behaviour assays. Experiments were conducted during the light cycle (7 a.m. to 7 p.m.). Mice were randomly assigned to experimental groups for specific behavioural assays immediately after surgery. Mice were habituated to investigator handling for 1–2 min on three consecutive days. Handling took place in the holding room where the mice were housed. Before each handling session, mice were transported by wheeled cart to and from the vicinity of the behaviour rooms to habituate them to the journey. For natural memory recall sessions, data were quantified using FreezeFrame software. Optogenetic stimulation interfered with the motion detection, and therefore all light-induced freezing behaviour was manually quantified. All behaviour experiments were analysed blind to experimental group. Unpaired Student's *t*-tests were used for independent group comparisons, with Welch's correction when group variances were significantly different. Given behavioural variability, initial assays were performed using a minimum of 10 mice per group to ensure adequate power for any observed differences. Experiments that resulted in significant behavioural effects were replicated three times in the laboratory. Following behavioural protocols, brain sections were prepared to confirm efficient viral labelling in target areas. Animals lacking adequate labelling were excluded before behaviour quantification.

Contextual fear conditioning. Two distinct contexts were employed[14]. Context A was 29 × 25 × 22 cm chambers with grid floors, opaque triangular ceilings, red lighting, and scented with 1% acetic acid. Four mice were run simultaneously in four identical context A chambers. Context B consisted of four 30 × 25 × 33 cm chambers with perspex floors, transparent square ceilings, bright white lighting, and scented with 0.25% benzaldehyde. All mice were conditioned in context A (two 0.60 mA shocks of 2 s duration in 5 min), and tested (3 min) in contexts A and B 1 day later. Experiments showed no generalization in the neutral context B. All experimental groups were counter-balanced for chamber within contexts. Floors of chambers were cleaned with quatricide before and between runs. Mice were transported to and from the experimental room in their home cages using a wheeled cart. The cart and cages remained in an anteroom to the experimental rooms during all behavioural experiments. For engram labelling, mice were kept on regular food without DOX for 24 h before training. When training was complete, mice were switched back to food containing 40 mg kg^{-1} DOX.

Open field. Spontaneous motor activity was measured in an open field arena (52 × 26 cm) for 10 min. All mice were transferred to the testing room and acclimated for 30 min before the test session. During the testing period, lighting in the room was turned off. The apparatus was cleaned with quatricide before and between runs. Total movements (distance travelled and velocity) in the arena were quantified using an automated infrared (IR) detection system (EthoVision XT, Noldus). The tracking software plotted heat maps for each mouse, which was averaged to create representative heat maps for each genotype. Raw data were extracted and analysed using Microsoft Excel.

Engram activation. For light-induced freezing behaviour, a context distinct from the CFC training chamber (context A) was used. These were 30 × 25 × 33 cm chambers with perspex floors, square ceilings, white lighting, and scented with 0.25% benzaldehyde. Chamber ceilings were customized to hold a rotary joint (Doric Lenses) connected to two 0.32-m patch cords. All mice had patch cords fitted to the optic fibre implant before testing. Two mice were run simultaneously in two identical chambers. ChR2 was stimulated at 20 Hz (15 ms pulse width) using a 473 nm laser (10–15 mW), for the designated epochs. Testing sessions were 12 min in duration, consisting of four 3 min epochs, with the first and third as light-off epochs, and the second and fourth as light-on epochs. At the end of 12 min, the mouse was detached and returned to its home cage. Floors of chambers were cleaned with quatricide before and between runs.

***In vivo* optical LTP.** One day after CFC training and engram labelling (DG plus PP terminals) in control and early AD groups, mice were placed in an open field arena (52 × 26 cm) after patch cords were fitted to the fibre implants. After a 15 min acclimatization period, mice with oChIEF$^+$ PP engram terminals in the DG received the optical LTP[23] protocol (100 blue light pulses of 2 ms each at a frequency of 100 Hz, repeated 5 times every 3 min). This *in vivo* protocol was repeated 10 times over a 3 h duration. After induction, mice remained in the arena for an additional 15 min before returning to their home cage. To apply optical LTP to a large portion of excitatory MEC neurons, an AAV virus expressing oChIEF-tdTomato under the CaMKII promoter, rather than a c-Fos-tTA/TRE virus (that is, engram labelling), was used. For protein synthesis inhibition experiments, immediately after the *in vivo* LTP induction protocol mice received 75 mg kg^{-1} anisomycin (Aniso) or an equivalent volume of saline intraperitoneally. Mice were then returned to their home cages. An hour later, a second injection of Aniso or saline was delivered.

Inhibitory avoidance. A 30 × 28 × 34 cm unscented chamber with transparent square ceilings and intermediate lighting was used. The chamber consisted of two sections, one with grid flooring and the other with a white light platform. During the conditioning session (1 min), mice were placed on the light platform, which is the less preferred section of the chamber (relative to the grid section). Once mice entered the grid section of the chamber (all four feet), 0.80 mA shocks of 2 s duration were delivered. On average, each mouse received 2–3 shocks per training session. After 1 min, mice were returned to their home cage. The next day, latency to enter the grid section of the chamber as well as total time on the light platform was measured (3 min test).

Novel object location. Spatial memory was measured in a white plastic chamber (28 × 28 cm) that had patterns (series of parallel lines or circles) on opposite walls. The apparatus was unscented and intermediate lighting was used. All mice were transferred to the behavioural room and acclimated for 30 min before the training session. On day 1, mice were allowed to explore the chamber with patterns for 15 min. On days 2 and 3, mice were introduced into the chamber that had an object (7-cm-tall glass flask filled with metal beads) placed adjacent to either patterned wall. The position of the object was counter-balanced within each genotype. On day 4, mice were placed into the chamber with the object either in the same position as the previous exposure (familiar) or at a novel location based on wall patterning. Frequency of visits to the familiar and novel object locations was quantified using an automated detection system (EthoVision XT, Noldus). Total time exploring the object was also measured (nose within 1.5 cm of object). The tracking software plotted heat maps based on exploration time, which was averaged to create representative heat maps for each genotype. Raw data were extracted and analysed using Microsoft Excel.

28. Reijmers, L. G., Perkins, B. L., Matsuo, N. & Mayford, M. Localization of a stable neural correlate of associative memory. *Science* **317,** 1230–1233 (2007).
29. Urlinger, S. *et al.* Exploring the sequence space for tetracycline-dependent transcriptional activators: novel mutations yield expanded range and sensitivity. *Proc. Natl Acad. Sci. USA* **97,** 7963–7968 (2000).

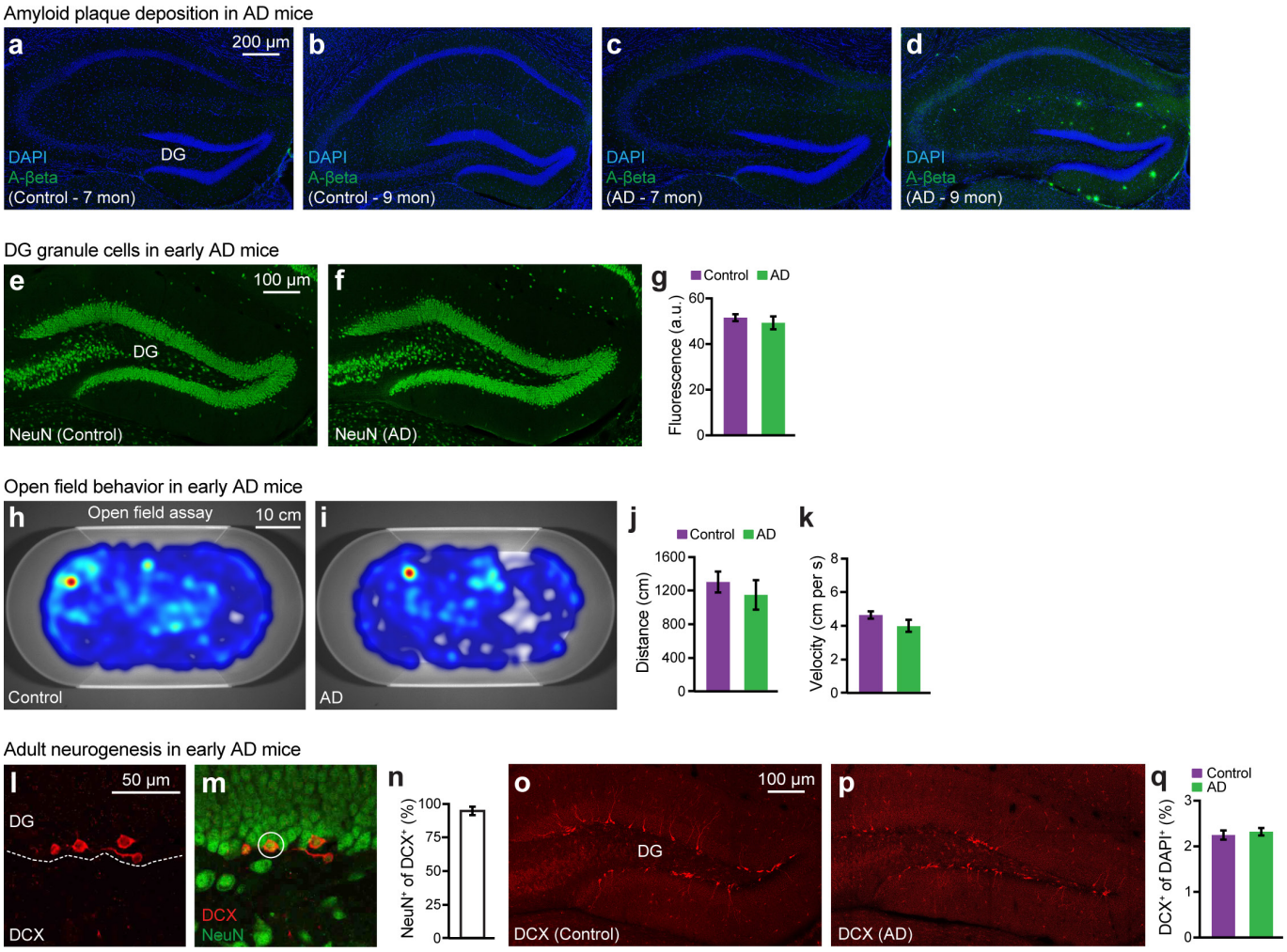

Extended Data Figure 1 | Characterization of 7-month-old early AD mice. **a**–**d**, Images showing hippocampal $A\beta^+$ plaques lacking in control mice (**a**, **b**) and 7-month-old AD mice (**c**), which showed an age-dependent increase in 9-month-old AD mice (**d**). **e**, **f**, Images showing neuronal nuclei (NeuN) staining of DG granule cells in control (**e**) and 7-month-old AD (**f**) mice. **g**, $NeuN^+$ fluorescence intensity of the granule cell layer from control and AD sections shown in **e**, **f** ($n = 8$ mice per group). **h**, **i**, Heat maps showing exploratory behaviour in an open field arena from control (**h**) and 7-month-old AD (**i**) mice. **j**, **k**, Distance travelled (**j**) and velocity (**k**) did not differ between control and AD groups ($n = 9$ mice per group). **l**, **m**, Images showing adult newborn neurons (DCX^+) in DG sections from control mice (**l**) that are double positive for NeuN (**m**). **n**, Percentage of $NeuN^+$ cells among DCX^+ cells ($n = 3$ mice). **o**, **p**, Images showing DCX^+ neurons in DG sections from control (**o**) and AD (**p**) groups ($n = 4$ mice per group). **q**, DCX^+ cell counts from control and AD mice. Data are presented as mean ± s.e.m.

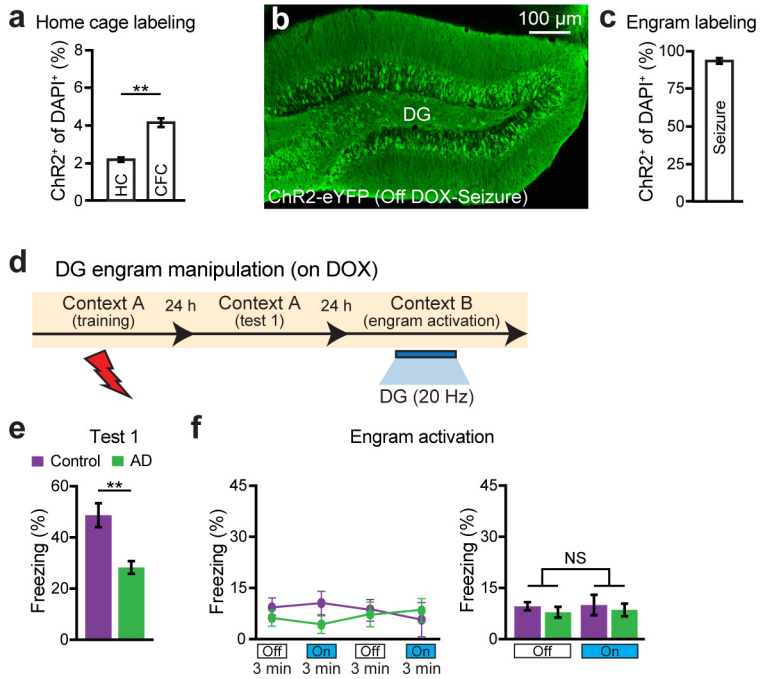

Extended Data Figure 2 | Labelling and engram activation of early AD mice on DOX. a, Mice are taken off DOX for 24 h in the home cage (HC) and subsequently trained in CFC. DG sections ($n = 3$ mice per group) revealed 2.05% ChR2–eYFP labelling in the home cage, consistent with the previously established engram tagging strategy[11]. **b**, Mice were injected with a virus cocktail of AAV_9-c-Fos-tTA and AAV_9-TRE-ChR2-eYFP. After 1 day off DOX, kainic acid was used to induce seizures. Image showing efficient labelling throughout the DG. **c**, ChR2–eYFP cell counts from DG sections shown in **b** ($n = 3$ mice). **d**, Behavioural schedule for optogenetic activation of DG engram cells. **e**, Memory recall 1 day after training (test 1) showed less freezing of AD mice compared with control mice ($n = 8$ mice per group). **f**, Engram activation with blue light stimulation (left). Average freezing for the two light-off and light-on epochs (right). Statistical comparisons are performed using unpaired *t*-tests; $^{**}P < 0.01$. Data are presented as mean ± s.e.m.

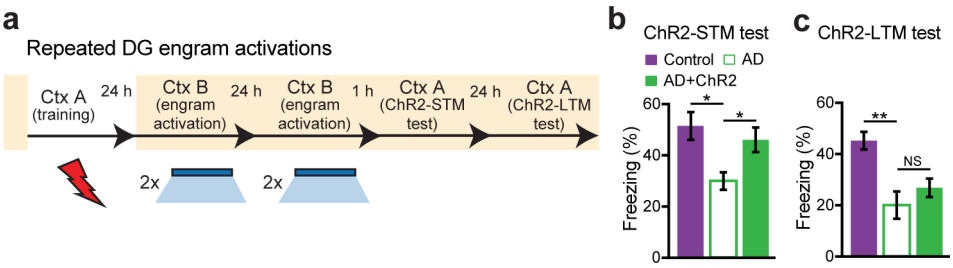

Extended Data Figure 3 | Chronic DG engram activation in early AD mice did not rescue long-term memory. a, Behavioural schedule for repeated DG engram activation experiment. Ctx, context. **b**, AD mice in which a DG memory engram was reactivated twice a day for 2 days (AD + ChR2) showed increased STM freezing levels compared with memory recall before engram reactivation (ChR2-STM test, $n = 9$ mice per group). **c**, Memory recall 1 day after repeated DG engram activations (ChR2-LTM test). NS, not significant. Statistical comparisons are performed using unpaired *t*-tests; $^{*}P < 0.05$, $^{**}P < 0.01$. Data are presented as mean ± s.e.m.

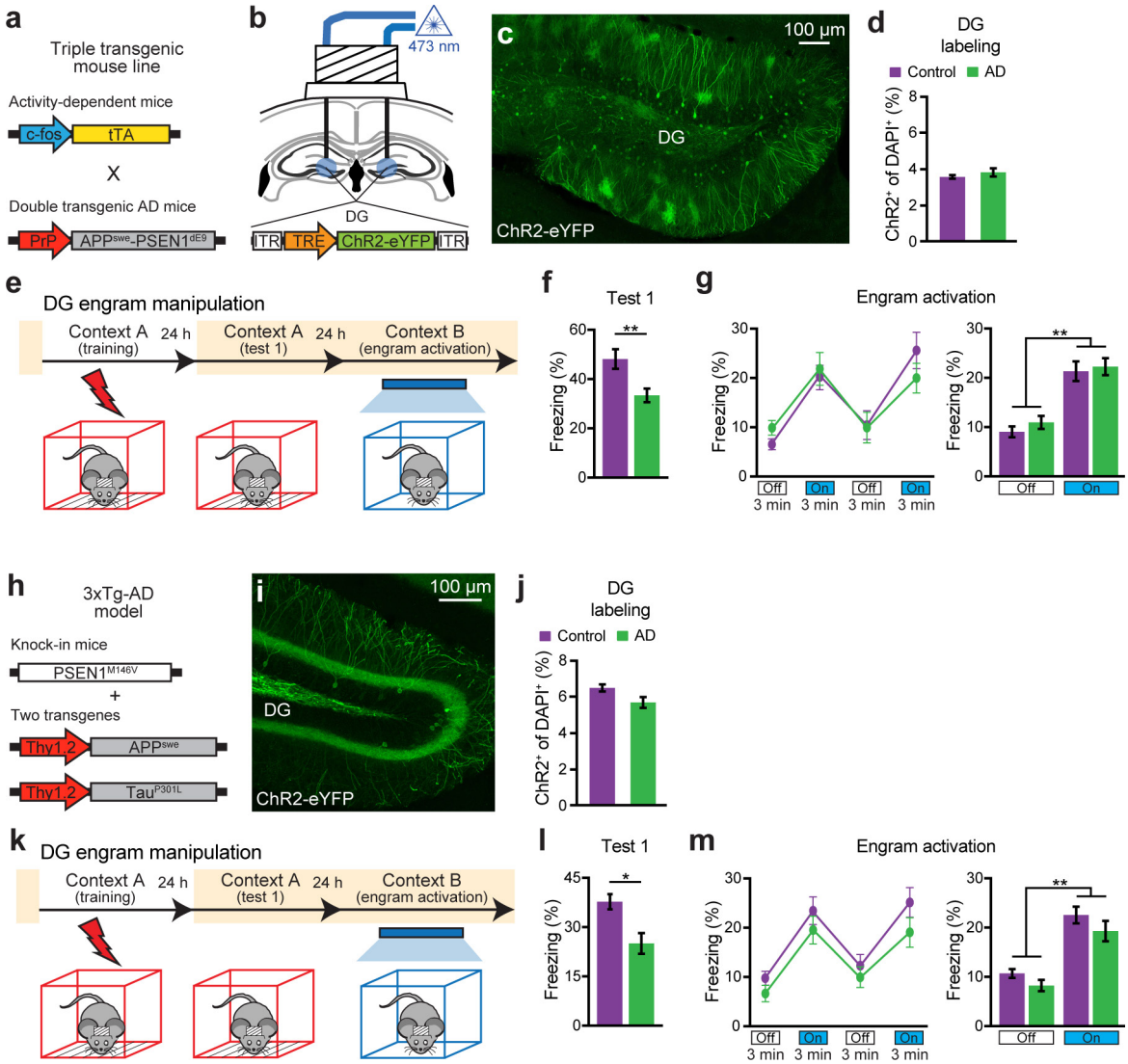

Extended Data Figure 4 | Engram activation restores fear memory in triple-transgenic and PS1/APP/tau models of early AD. a, Triple-transgenic mouse line obtained by mating *c-Fos-tTA* transgenic mice[11,28] with double-transgenic APP/PS1 AD mice[10]. These mice combined with a DOX-sensitive AAV virus permits memory engram labelling in early AD. **b**, Triple-transgenic mice were injected with AAV_9-TRE-ChR2-eYFP and implanted with an optic fibre targeting the DG. **c**, Image showing DG engram cells of triple-transgenic mice 24 h after CFC. **d**, ChR2–eYFP cell counts from control and triple-transgenic AD mice ($n = 5$ mice per group). **e**, Behavioural schedule for engram activation. **f**, Memory recall 1 day after training (test 1) showed less freezing of triple-transgenic AD mice compared with control mice ($n = 10$ mice per group). **g**, Engram activation with blue light stimulation (left). Average freezing for the two light-off and light-on epochs (right). **h**, Triple-transgenic AD model (3×Tg-AD) as previously reported[18]. A cocktail of AAV_9-c-Fos-tTA and AAV_9-TRE-ChR2-eYFP viruses were used to label memory engrams in 3×Tg-AD mice. **i**, Image showing memory engram cells in the DG of 3× Tg-AD mice 24 h after CFC. **j**, ChR2–eYFP cell counts from DG sections of control and 3×Tg-AD mice ($n = 4$ mice per group). **k**, Behavioural schedule for engram activation. **l**, Memory recall 1 day after training (test 1) showed less freezing of 3×Tg-AD mice compared with control mice ($n = 9$ mice per group). **m**, Engram activation with blue light stimulation (left). Average freezing for the two light-off and light-on epochs (right). Statistical comparisons are performed using unpaired *t*-tests; $^*P < 0.05$, $^{**}P < 0.01$. Data are presented as mean ± s.e.m.

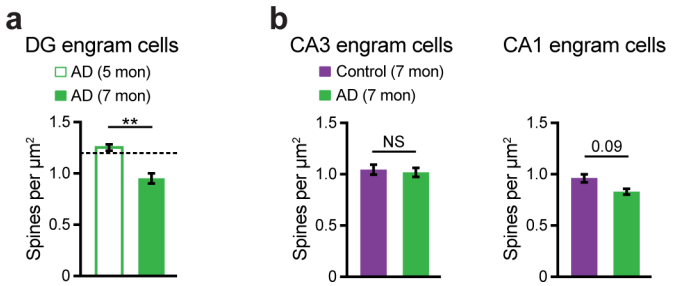

Extended Data Figure 5 | Dendritic spines of engram cells in 7-month-old early AD mice. a, Average dendritic spine density of DG engram cells showed an age-dependent decrease in 7-month-old APP/PS1 AD mice ($n = 7{,}032$ spines) as compared to 5-month-old AD mice ($n = 4{,}577$ spines, $n = 4$ mice per group). Dashed line represents spine density of control mice (1.21). **b**, Left, average dendritic spine density of CA3 engram cells in control ($n = 5{,}123$ spines) and AD mice ($n = 6{,}019$ spines, $n = 3$ mice per group). Right, average dendritic spine density of CA1 engram cells in control ($n = 9{,}120$ spines) and AD mice ($n = 7{,}988$ spines, $n = 5$ mice per group). NS, not significant. Statistical comparisons are performed using unpaired *t*-tests; $^{**}P < 0.01$. Data are presented as mean ± s.e.m.

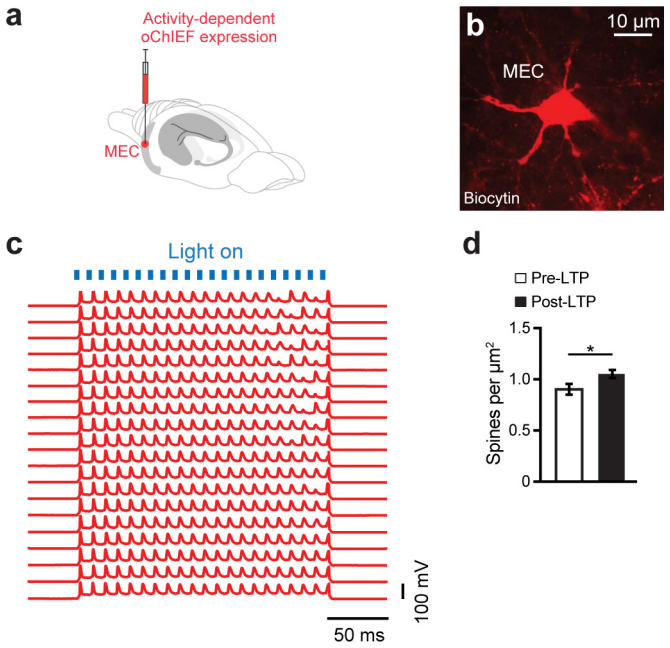

Extended Data Figure 6 | High-fidelity responses of oChIEF$^+$ cells and dendritic spines of DG engram cells after *in vitro* optical LTP. **a**, EC cells were injected with a virus cocktail containing AAV$_9$-TRE-oChIEF-tdTomato for activity-dependent labelling. **b**, Image showing a biocytin-filled oChIEF$^+$ stellate cell in the EC. **c**, 100 Hz (2-ms pulse width) stimulation of an oChIEF$^+$ cell across 20 consecutive trials. Spiking responses exhibit high fidelity. **d**, Average dendritic spine density of biocytin-filled DG cells showed an increase after optical LTP induction *in vitro* ($n = 1{,}452$ spines, $n = 6$ cells). Statistical comparisons are performed using unpaired *t*-tests; $^*P < 0.05$. Data are presented as mean ± s.e.m.

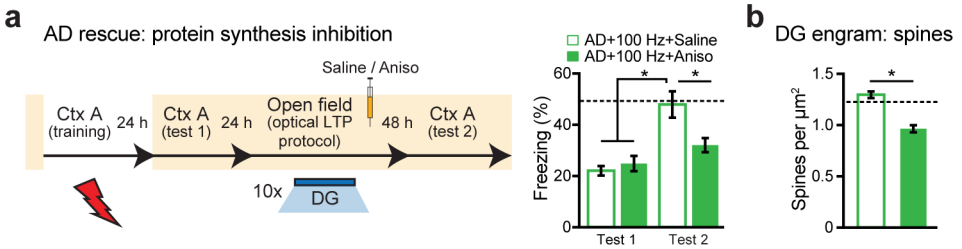

Extended Data Figure 7 | Behavioural rescue and spine restoration by optical LTP is protein-synthesis dependent. a, Modified behavioural schedule for long-term rescue of memory recall in AD mice in the presence of saline or anisomycin (left). Memory recall 2 days after LTP induction followed by drug administration showed less freezing of AD mice treated with anisomycin (AD + 100 Hz + Aniso) compared with saline-treated AD mice (AD + 100 Hz + saline, $n = 9$ mice per group; right). Dashed line represents freezing level of control mice (48.53). Ctx, context. **b**, Average dendritic spine density in early AD mice treated with anisomycin after LTP induction ($n = 4{,}810$ spines) was decreased compared with saline-treated AD mice ($n = 6{,}242$ spines, $n = 4$ mice per group). Dashed line represents spine density of control mice (1.21). Statistical comparisons are performed using unpaired t-tests; $^*P < 0.05$. Data are presented as mean ± s.e.m.

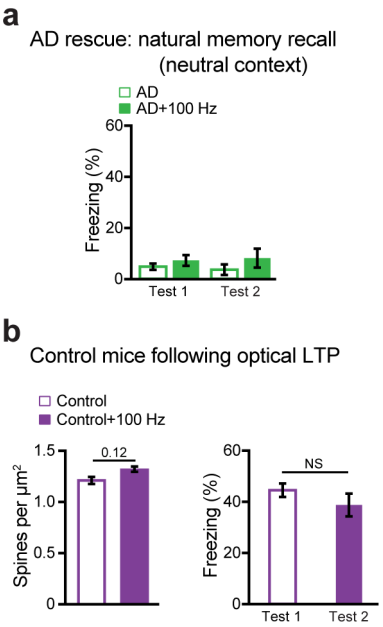

Extended Data Figure 8 | Rescued early AD mouse behaviour in a neutral context and control mouse behaviour after *in vivo* optical LTP. **a**, After the long-term rescue of memory recall in AD mice (test 2; Fig. 3m), animals were placed in an untrained neutral context to measure generalization ($n = 10$ mice per group). Rescued AD mice (AD + 100 Hz) did not display freezing behaviour. **b**, Left, average dendritic spine density of DG engram cells from control mice remained unchanged after optical LTP induction *in vivo* (control + 100 Hz, $n = 4{,}211$ spines, $n = 3$ mice; control data from Fig. 2c). Right, the behavioural rescue protocol applied to early AD mice (Fig. 3m) was tested in age-matched control mice ($n = 9$ mice per group). Similar freezing levels were observed after optical LTP (test 2) as compared to memory recall before the 100 Hz protocol (test 1). NS, not significant. Statistical comparisons are performed using unpaired *t*-tests. Data are presented as mean ± s.e.m.

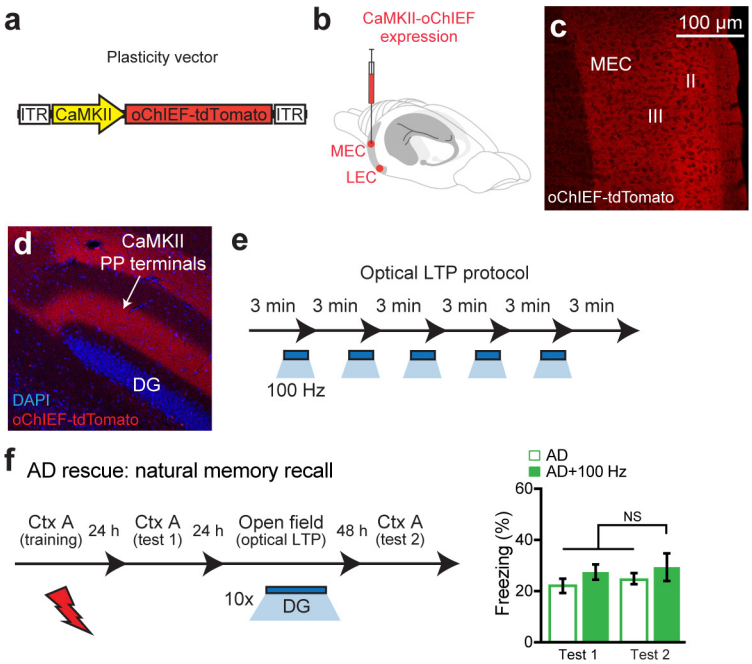

Extended Data Figure 9 | Optical LTP using a CaMKII-oChIEF virus did not rescue memory in early AD mice. a, AAV virus expressing oChIEF-tdTomato under a CaMKII promoter. **b**, CaMKII-oChIEF virus injected into MEC and LEC. **c**, **d**, Images showing tdTomato labelling in a large portion of excitatory MEC neurons (**c**) as well as the PP terminals in the DG (**d**). **e**, *In vivo* optical LTP protocol[23]. **f**, Behavioural schedule for long-term rescue of memory recall in AD mice (left). In contrast to the engram-specific strategy, long-term memory could not be rescued by stimulating a large portion of excitatory PP terminals in the DG (right; $n = 9$ mice per group). NS, not significant. Statistical comparisons are performed using unpaired *t*-tests. Data are presented as mean ± s.e.m.

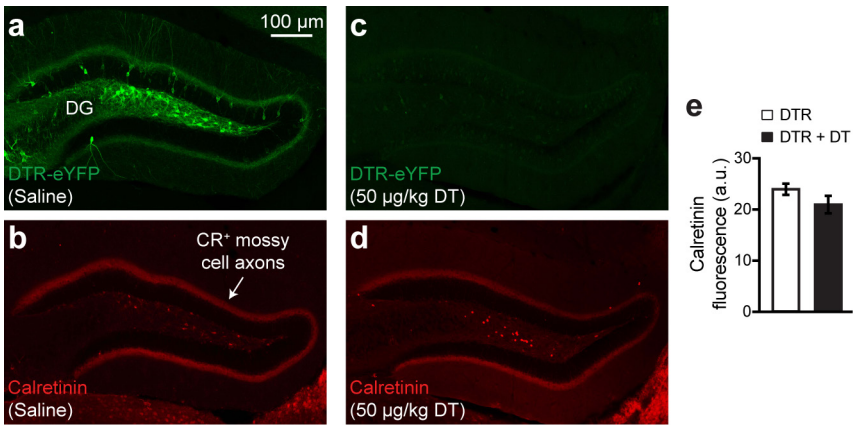

Extended Data Figure 10 | Normal DG mossy cell density after engram cell ablation. a–d, Images showing DG engram cells after saline treatment (**a**) and the corresponding calretinin positive (CR^+) mossy cell axons (**b**). DTR–eYFP engram cell labelling after DT treatment (**c**) and the respective CR^+ mossy cell axons (**d**). **e**, CR^+ fluorescence intensity of mossy cell axons from saline- and DT-treated DG sections shown in **a–d** ($n = 8$ mice per group). Data are presented as mean ± s.e.m.